

# Design and High-Resolution Structure of a $\beta^3$ -Peptide Bundle Catalyst

Pam S. P. Wang,<sup>†</sup> Jennifer B. Nguyen,<sup>†</sup> and Alanna Schepartz<sup>\*,†,‡</sup>

<sup>†</sup>Department of Chemistry and <sup>‡</sup>Department of Molecular, Cellular and Developmental Biology, Yale University, New Haven, Connecticut 06520-8107, United States

**S** Supporting Information

**ABSTRACT:** Despite the widespread exploration of  $\alpha$ -peptides as catalysts, there are few examples of  $\beta$ -peptides that alter the course of a chemical transformation. Our previous work demonstrated that a special class of  $\beta^3$ -peptides spontaneously self-assembles in water into discrete protein-like bundles possessing unique quaternary structures and exceptional thermodynamic stability. Here we describe a series of  $\beta^3$ -peptide bundles capable of both substrate binding and chemical catalysis—ester hydrolysis. A combination of kinetic and high-resolution structural analysis suggests an active site triad composed of residues from at least two strands of the octameric bundle structure.

Peptides embody two molecular properties that engender chemical catalysis. The propensity of a polyamide backbone, even a short one, to occupy a restricted conformational space facilitates the judicious placement of potential catalytic, recognition, or stabilizing groups, while the chirality of amino acid monomers and the structures they form can impart intrinsic selectivity. Despite the widespread exploration of  $\alpha$ -peptides as catalysts for numerous reactions,<sup>1</sup> there are only two reported examples of  $\beta$ -peptides that alter the course of a chemical transformation.<sup>2</sup>  $\beta$ -Peptides are polymers of  $\beta$ -amino acids, which differ from natural  $\alpha$ -amino acids by the addition of a single backbone methylene unit per residue; the additional methylene unit imparts structural and metabolic stability.<sup>3</sup>

Our previous work demonstrated that a special class of  $\beta^3$ -peptides self-assembles in water into discrete helical bundles possessing a protein-like tertiary fold and exceptionally high thermodynamic stability.<sup>4</sup> Here we report a series of  $\beta^3$ -peptide bundles capable of both substrate binding and chemical catalysis—ester hydrolysis. A combination of kinetic and high-resolution structural analysis suggests an esterase active site composed of three functional groups positioned on separate strands of the octameric bundle structure.

Our design began with the structure of Zwit-EYYK, the most thermally and kinetically stable  $\beta^3$ -peptide bundle characterized to date.<sup>4d</sup> The Zwit-EYYK bundle folds cooperatively ( $T_M = 78$  °C at 25  $\mu$ M) and is >90% octameric at this concentration.<sup>4d</sup> As a model reaction, we chose the hydrolysis of 8-acetoxypyrene-1,3,6-trisulfonate (**1**), which releases the fluorescent product pyranine (**2**) upon ester hydrolysis (Figure 1A). Previous work has shown that arginine side chains in natural enzymes can interact favorably with sulfonate groups; the binding of coenzyme M to hydrogenases is one example of such an

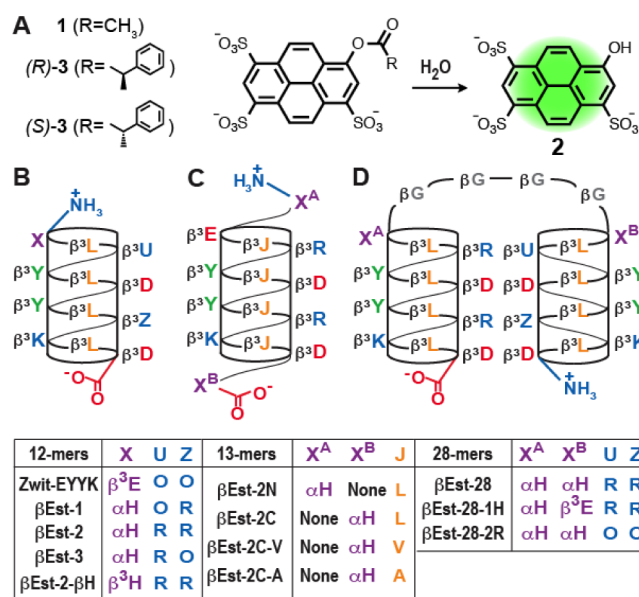


**Figure 1.** (A) Reactions evaluated in the presence or absence of the  $\beta^3$ -peptides shown in panels B–D. Not all sequences assemble into  $\beta^3$ -peptide bundles (see text). (B–D) Helical net diagrams of  $\beta^3$ -peptides studied herein.

interaction.<sup>5</sup> Previous work has also shown that histidine side chains are used extensively within the active sites of natural esterases, either as nucleophiles or, more frequently, as general acids/bases.<sup>6</sup> There is also an extensive biomimetic chemistry literature<sup>7</sup> to support combining binding and catalytic groups to facilitate chemical reactions in aqueous solution. We sought to test the hypothesis that a  $\beta^3$ -peptide bundle endowed with judiciously positioned arginine and histidine side chains would catalyze the hydrolysis of **1**.

To test this hypothesis, we modified the sequence of the Zwit-EYYK monomer to electrostatically guide substrate **1** into the proximity of a single histidine side chain while minimally perturbing the bundle structure. Substrate **1** is planar, with three sulfonate groups whose structural relationship mimics that between side chains at positions  $i$  and  $i + 6$  on a single 14-helix face. We reasoned that substituting arginine for the ornithine at positions 3 and 9 of Zwit-EYYK (U and Z in Figure 1B) would facilitate electrostatic guidance<sup>8</sup> to a histidine side chain at

Received: February 9, 2014

Published: May 6, 2014

position 1 (X in Figure 1B) without severely compromising bundle stability. A similar logic has been previously applied to design a cyclic peptide catalyst for an analogous ester substrate.<sup>9</sup> Based on this design rationale, we synthesized three variants of Zwit-EYYK carrying a single  $\alpha$ -histidine ( $\alpha$ H) at position 1 and one or two  $\beta^3$ -homoarginine ( $\beta^3$ R) residues at positions 3 and 9 (Figure 1B).<sup>10</sup> Preliminary data showed that all three of these first-generation peptides— $\beta$ Est-1,  $\beta$ Est-2, and  $\beta$ Est-3—catalyzed the hydrolysis of 1 mM substrate 1 at a catalyst loading of 10 mol% in a solution buffered at pH 6, increasing the background reaction rate by a factor of 20–30. Zwit-EYYK, as expected, was inactive, while free histidine at 10 mol% enhanced the reaction rate by <5-fold (Figure S1).

We next performed steady-state measurements to characterize the reaction kinetics in greater detail. Incubation of 25  $\mu$ M  $\beta^3$ -peptide ( $\beta$ Est-1,  $\beta$ Est-2 or  $\beta$ Est-3) with 0.15–2.5 mM 1 revealed that hydrolysis followed Michaelis–Menten kinetics (Figure 2A). Kinetic constants derived from these data suggested  $k_{\text{cat}}$

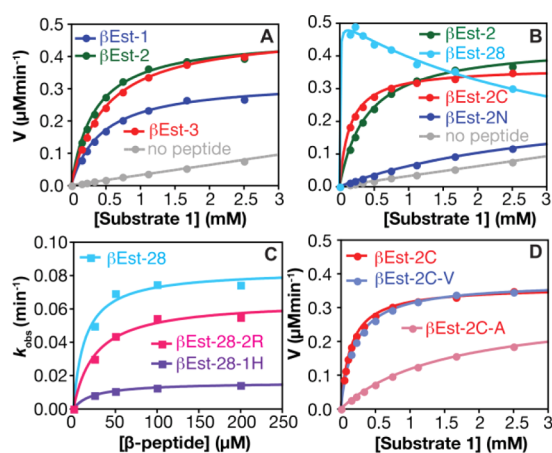


**Figure 2.** (A,B,D) Plots of observed initial reaction rate ( $V$ ) vs substrate 1 concentration in the absence or presence of the indicated  $\beta^3$ -peptide. Data were fit to the Michaelis–Menten equation; panel B also shows the fit to the Haldane equation (cyan,  $\beta$ Est-28), which accounts for substrate inhibition. Reactions were performed in a 10 mM Bis-Tris buffer (pH 6) with [ $\beta^3$ -peptide] = 25  $\mu$ M. (C) Plots of  $k_{\text{obs}}$  vs [ $\beta^3$ -peptide] measured under pre-steady-state conditions.

values of 0.013, 0.018, and 0.019  $\text{min}^{-1}$  and  $K_M$  values of 447, 345, and 487  $\mu$ M for  $\beta$ Est-1,  $\beta$ Est-2, and  $\beta$ Est-3, respectively.  $\beta$ Est-2, containing two  $\beta^3$ R residues, displayed a more favorable  $K_M$  and the highest specificity ( $k_{\text{cat}}/K_M = 54 \text{ M}^{-1} \text{ min}^{-1}$ ). Since  $K_M$  reflects binding affinity, this observation supports a model in which substrate binding is mediated by electrostatic interactions between guanidinium groups on the peptide and sulfonate groups on the substrate. Relative to the buffer reaction,  $\beta$ Est-1,  $\beta$ Est-2, and  $\beta$ Est-3 enhanced the rate of ester hydrolysis ( $k_{\text{cat}}/k_{\text{uncat}}$ ) by factors of 413, 588, and 612. These kinetic parameters are comparable to those of a similarly sized dendritic peptide, RM-G2, which catalyzes the hydrolysis of 1 with a rate enhancement of 340 and  $k_{\text{cat}}/K_M = 120 \text{ M}^{-1} \text{ min}^{-1}$  at pH 5.5.<sup>7e</sup> In a similar way, a designed 4-helix  $\alpha$ -peptide bundle, MNKR, catalyzes *p*-nitrophenyl fumarate ester hydrolysis with  $k_{\text{cat}}/K_M = 10.2 \text{ M}^{-1} \text{ min}^{-1}$  at pH 5.<sup>7f</sup> The only other 14-helical  $\beta$ -peptide catalyst reported, whose structure is unknown, catalyzes the retroaldol cleavage of a  $\beta$ -hydroxyketone with  $k_{\text{cat}}/K_M = 26 \text{ M}^{-1} \text{ min}^{-1}$  despite a rate acceleration of  $k_{\text{cat}}/k_{\text{uncat}} = 3000$ .<sup>2a</sup>

The favorable kinetic constants notwithstanding, subsequent circular dichroism experiments revealed that while  $\beta$ Est-1,  $\beta$ Est-

2, and  $\beta$ Est-3 assembled into bundles at high concentration, they were primarily monomeric at 25  $\mu$ M, the concentration chosen for steady-state kinetics (Figure S2). Compared to Zwit-EYYK, which was >90% octameric at 25  $\mu$ M,  $\beta$ Est-1,  $\beta$ Est-2, and  $\beta$ Est-3 were <30% assembled at this concentration. The Zwit-EYYK X-ray structure revealed that the  $\beta^3$ E at position 1 (X in Figure 1B) is involved in an interhelical salt-bridge interaction. This side chain is substituted by  $\alpha$ H in  $\beta$ Est-1– $\beta$ Est-3, suggesting that the observed destabilization could be due to loss of this acidic side chain or inclusion of an  $\alpha$ -amino acid at this position, or a combination of these effects.<sup>4d</sup>

We pursued three strategies to recover bundle stability. To evaluate whether the decrease in stability resulted from the presence of an  $\alpha$ -amino acid ( $\alpha$ H) at position 1, we synthesized a variant of  $\beta$ Est-2 that contained  $\beta^3$ H at this position ( $\beta$ Est-2- $\beta$ H in Figure 1B). To evaluate whether the decrease was due to loss of  $\beta^3$ E at position 1, we restored this residue and appended the  $\alpha$ H to either the N- or C-terminus as a 13th residue ( $\beta$ Est-2N and  $\beta$ Est-2C in Figure 1C). Finally, to evaluate whether entropic effects could be harnessed to improve bundle stability, we synthesized a covalent dimer containing two  $\beta$ Est-2 monomers joined with a tetra- $\beta$ -homoglycine ( $\beta$ G) linker, an analogue of the highly stable Z28 bundle reported previously ( $\beta$ Est-28 in Figure 1D).<sup>11</sup>

The kinetic constants in Table 1 reveal dimerization as the most effective strategy to regain bundle structure and improve

**Table 1. Kinetic Constants Characterizing the Hydrolysis of 1 by  $\beta^3$ -Peptide Catalysts**

peptide	$k_{\text{cat}}$ ( $\text{min}^{-1}$ )	$K_M$ ( $\mu\text{M}$ )	$k_{\text{cat}}/K_M$ ( $\text{M}^{-1} \text{ min}^{-1}$ )	$k_{\text{cat}}/k_{\text{uncat}}^a$	bundle at 25 $\mu\text{M}$ ?
$\beta$ Est-1	0.013	447	29	413	no
$\beta$ Est-2	0.018	345	54	588	no
$\beta$ Est-3	0.019	487	39	612	no
$\beta$ Est-2- $\beta$ H	0.008	351	23	255	yes
$\beta$ Est-2N	0.011	3467	3	356	yes
$\beta$ Est-2C	0.014	147	98	460	yes
$\beta$ Est-28 <sup>b</sup>	0.020	4	5102	649	yes
$\beta$ Est-28-1H <sup>b</sup>	0.014	14	1028	458	yes
$\beta$ Est-28-2R <sup>b</sup>	0.026	4	6446	820	yes
$\beta$ Est-2C-V	0.015	204	73	476	yes
$\beta$ Est-2C-A	0.012	1602	8	386	no

<sup>a</sup> $k_{\text{uncat}} = 3.144 \times 10^{-5} \text{ min}^{-1}$ . <sup>b</sup>Constants calculated using the Haldane equation to account for substrate inhibition. To aid comparisons, kinetic constants were calculated on the basis of moles of  $\beta^3$ -peptide, not moles of  $\beta^3$ -peptide bundle.

catalytic activity. While  $\beta$ Est-2- $\beta$ H was more structured than  $\beta$ Est-2 (almost 80% bundle at 25  $\mu$ M), its esterase activity was compromised, with  $k_{\text{cat}}/K_M = 23 \text{ M}^{-1} \text{ min}^{-1}$  (Figure S3). In a similar way,  $\beta$ Est-2N,  $\beta$ Est-2C, and  $\beta$ Est-28 all exhibited higher degrees of association (>80% bundle at 25  $\mu$ M) than  $\beta$ Est-2 (Figure S4). However, the catalytic activities of these peptides varied drastically:  $\beta$ Est-2C was more efficient than  $\beta$ Est-2,  $\beta$ Est-2N was virtually inactive, and  $\beta$ Est-28 displayed very rapid initial rates but did not obey Michaelis–Menten kinetics (Figure 2B). The dependence of catalytic activity on the relative positions of  $\alpha$ H and  $\beta^3$ R residues implies that peptide–substrate interactions are highly specific. The nearly 2-fold increase in the catalytic efficiency of  $\beta$ Est-2C ( $k_{\text{cat}}/K_M = 98 \text{ M}^{-1} \text{ min}^{-1}$ ) over  $\beta$ Est-2 ( $k_{\text{cat}}/K_M = 54 \text{ M}^{-1} \text{ min}^{-1}$ ) is a result of its improved affinity for the substrate ( $K_M = 147 \mu\text{M}$ ) and perhaps the enhanced helicity

of  $\beta$ Est-2C at 25  $\mu$ M. The nearly 100-fold increase in the catalytic efficiency of  $\beta$ Est-28 is also the result of a greatly improved substrate affinity ( $K_M = 4 \mu$ M).

We designed  $\beta$ Est-28 using a previously reported strategy that recapitulates the characteristic  $\beta^3$ -peptide octamer fold with 4 subunits instead of 8.<sup>11</sup> Although the relative positions of the  $\alpha$ H and the  $\beta^3$ R residues in  $\beta$ Est-28 mimic those in  $\beta$ Est-2, the kinetic profile of  $\beta$ Est-28 was entirely unanticipated. Instead of initial velocity ( $V$ ) increasing as a function of substrate concentration,  $V$  reached a maximum at  $[1] = 200 \mu$ M and then steadily descended toward an asymptote. This behavior is diagnostic of substrate inhibition, a well-known phenomenon that occurs in  $\sim 20\%$  of natural enzymes, often to avoid excessive production or degradation of important metabolic intermediates.<sup>12</sup> We used the Haldane equation<sup>13</sup>—a modified version of the Michaelis–Menten equation that includes an additional equilibrium constant,  $K_i$ —to fit the hydrolysis kinetics observed in the presence of  $\beta$ Est-28. The Haldane model calculates  $k_{cat}/K_M = 5102 \text{ M}^{-1} \text{ min}^{-1}$  for  $\beta$ Est-28, almost 2 orders of magnitude greater than that for  $\beta$ Est-2.  $\beta$ Est-28 is 85% bundle at 25  $\mu$ M concentration, emphasizing the benefit of a catalyst possessing higher order structure and multiple potential catalytic sites.

To provide additional support for the substrate inhibition model, we conducted kinetic measurements under pre-steady-state conditions. These measurements were performed using excess  $\beta$ Est-28 (5- to 40-fold over substrate 1), which allowed us to monitor a single substrate turnover. Because the substrate was present in such small amounts relative to  $\beta$ Est-28, the possibility of substrate inhibition was effectively excluded. The observed rate constants,  $k_{obs}$ , were extracted from fits of the data at each catalyst concentration to single-exponential curves (Figure S5). A plot of  $k_{obs}$  against catalyst concentration (Figure 2C) was then fit to a hyperbolic function to obtain the rate constant for the chemical step,  $k_{chem}$  (the horizontal asymptote), and the apparent  $K_d$  (the peptide concentration corresponding to half of the asymptote). The kinetic parameters obtained from pre-steady-state studies of  $\beta$ Est-28 ( $k_{chem} = 0.083 \text{ min}^{-1}$ ;  $K_{d,app} = 14 \mu$ M) agreed well with those obtained from steady-state measurements ( $k_{cat} = 0.020 \text{ min}^{-1}$ ;  $K_M = 4 \mu$ M), providing support for the substrate inhibition model.  $k_{chem}$  is expected to be equal to or greater than  $k_{cat}$ , since the latter is reflective of the rate-limiting step of the reaction. On the other hand,  $K_{d,app}$  should closely match  $K_M$ , since both reflect the affinity of the catalyst for the substrate.<sup>14</sup>

One explanation for the substrate inhibition observed with  $\beta$ Est-28 is that, as a covalently linked dimer of  $\beta$ Est-2, it contains 4  $\beta^3$ R and 2  $\alpha$ H residues, increasing the likelihood of alternative, nonproductive catalyst–substrate interactions. To investigate this possibility, we synthesized two  $\beta$ Est-28 variants, one containing a single  $\alpha$ H per  $\beta$ Est-28 monomer and another containing a single pair of  $\beta^3$ R residues per  $\beta$ Est-28 monomer ( $\beta$ Est-28-1H and  $\beta$ Est-28-2R in Figure 1D, respectively).  $\beta$ Est-28-1H was 5-fold less active than  $\beta$ Est-28, with changes in both  $k_{cat}$  and  $K_M$ . Surprisingly,  $\beta$ Est-28-2R is (slightly) more active than  $\beta$ Est-28. Substrate inhibition was observed in both cases (Figure S6), suggesting that further studies will be necessary to completely understand the origins of this effect. Pre-steady-state analyses reveal, nevertheless, that the additional  $\alpha$ H and  $\beta^3$ R residues enhance catalyst efficiency in a single substrate turnover; as assessed by the metrics  $k_{chem}$  and  $K_{d,app}$ , neither of the two 28-mer variants was as active as the parent  $\beta$ Est-28 (Figure 2C).

We next investigated the dependence of catalytic activity on  $\beta^3$ -peptide bundle stoichiometry. As previously reported, there

exists a direct relationship between bundle stoichiometry and  $\beta^3$ -peptide sequence; specifically,  $\beta^3$ -peptides with  $\beta^3$ L residues at positions  $i$ ,  $i+3$ ,  $i+6$ , and  $i+9$  assemble into octamers, those with  $\beta^3$ V or  $\beta^3$ I at these positions assemble into tetramers, and those with  $\beta^3$ A at these positions are constitutively monomeric.<sup>15</sup> Based on this relationship, we synthesized two stoichiometric variants of  $\beta$ Est-2C, one containing an all-valine face and another containing an all-alanine face ( $\beta$ Est-2C-V and  $\beta$ Est-2C-A in Figure 1C, respectively). Steady-state kinetics measurements revealed that the monomeric  $\beta$ Est-2C-A was the least effective catalyst of this series (Figure 2D), while  $\beta$ Est-2C and  $\beta$ Est-2C-V (80% and 73% bundle at 25  $\mu$ M) exhibited similar levels of activity. These results support the conclusions that bundle formation contributes to catalysis and that octamers and tetramers, but not monomers, can assemble a functional esterolytic active site.

To understand the differences in activity between bundle-forming and monomeric  $\beta^3$ -peptide catalysts, we obtained a high-resolution X-ray structure of  $\beta$ Est-2C. As predicted,  $\beta$ Est-2C self-associates into a quaternary assembly whose backbone skeleton is virtually superimposable with that of the Zwit-EYYK octamer (RMSD = 0.171; SDM at 5.0  $\text{\AA}$  cutoff = 3.425; Q-score = 0.920) (Figure 3A). The refined model of the  $\beta$ Est-2C bundle at 1.81  $\text{\AA}$

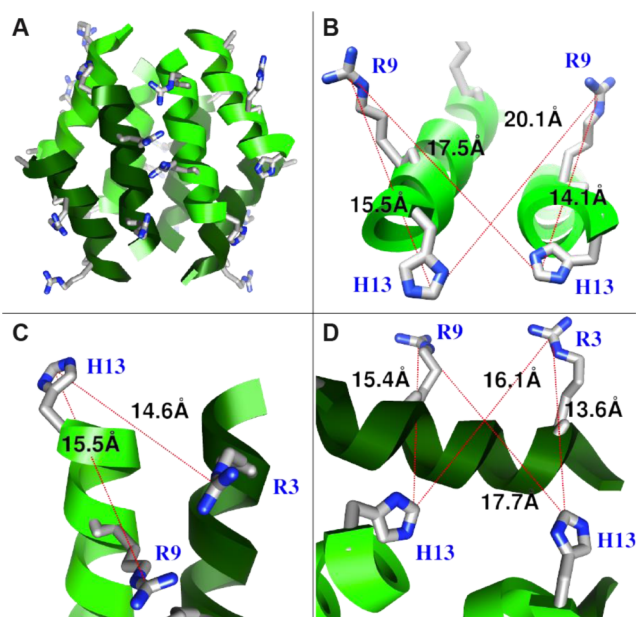


**Figure 3.** Structure of the  $\beta$ Est-2C bundle at 1.81  $\text{\AA}$  resolution. Shading corresponds to helix orientation. (A) Ribbon diagram of a single octamer showing the  $\alpha$ H and  $\beta^3$ R side chains (gray). (B–D) Representative interhelical active sites at the (B) parallel, (C) antiparallel, and (D) tetramer–tetramer interfaces. Distances between histidine and arginine side chains are highlighted in red.

resolution ( $R/R_{free} = 21.1/24.6\%$ ) consists of eight 14-helices organized into two tetramers related by a two-fold rotation axis, with each tetramer comprising four helices arranged in a parallel/antiparallel/parallel array. Substituting arginine for ornithine side chains retained the salt-bridge interactions, and interestingly, some interhelical arginine residues are parallel-stacked, a configuration that is often present within highly polar networks in natural proteins.<sup>16</sup> Additionally, the C-terminal histidines  $\pi$ -stack with adjacent tyrosine side chains at the tetramer–tetramer interface.

But how many potential active sites does the  $\beta$ Est-2C bundle contain? The dimensions of substrate **1** (7.4 Å long, 5.4 Å wide) suggest that an active site on the  $\beta$ Est-2C bundle would be characterized by one  $\alpha$ H and two  $\beta^3$ R residues located within roughly 15–20 Å. Taken with the structure, this analysis suggests that the  $\beta$ Est-2C bundle contains three fundamentally different active sites. The first occurs at the parallel interhelical interface and consists of a  $\beta^3$ R<sub>9</sub>– $\alpha$ H<sub>13</sub> side-chain pair from one helix and a  $\beta^3$ R<sub>9</sub> side chain from an adjacent helix (Figure 3B). The second potential active site, which occurs at an antiparallel interhelical interface, contains the same  $\beta^3$ R<sub>9</sub>– $\alpha$ H<sub>13</sub> pair but includes  $\beta^3$ R<sub>3</sub> from the neighboring helix (Figure 3C). The third potential active site is located at the tetramer–tetramer interface, consisting of  $\alpha$ H<sub>13</sub> from one helix and a  $\beta^3$ R<sub>3</sub>– $\beta^3$ R<sub>9</sub> pair from another (Figure 3D). Considering that each bundle comprises 4 parallel, 2 antiparallel, and 4 tetramer–tetramer helical contacts, and there are 2 active sites per interhelical interface, there are theoretically 20 intermolecular active sites per bundle. This analysis could explain the observation that bundle assembly enhances catalysis, even assuming low active-site occupancy.

Finally, we asked whether intrinsic chirality would endow  $\beta^3$ -peptide bundles with the ability to effect enantioselective catalysis. Indeed,  $\beta$ Est-2C exhibited significant chiral discrimination between the enantiomers of the 2-phenylpropionate ester substrate (*R*)-**3** and (*S*)-**3**, catalyzing the hydrolysis of (*R*)-**3** 4 times faster than that of (*S*)-**3** at 10 mol% catalyst loading (Figure S7). Although the selectivity of  $\beta$ Est-2C is modest in comparison to that of natural enzymes, it compares favorably with other synthetic esterases demonstrating activity on similar substrates. One dendritic peptide, for example, favors the enantiomer (*S*)-**3** with an enantiomeric ratio  $E = 2.8$ .<sup>7h</sup> This result, together with the kinetic parameters of the peptides we evaluated, suggests that  $\beta^3$ -peptide bundles are no less desirable than  $\alpha$ -peptides as scaffolds for catalyst development and may have unique advantages due to the combined attributes of structural predictability, stability, and metabolic orthogonality.

In summary, here we describe a structurally characterized  $\beta^3$ -peptide bundle possessing measurable catalytic function. Unlike two previously reported  $\beta$ -peptide catalysts,<sup>2</sup> the molecules described here self-assemble into discrete, unique, thermostable quaternary structures and are capable of both substrate recognition and chemical catalysis. The dependence of catalytic activity on the geometric arrangement of histidine and arginine residues, as well as bundle assembly, points to the existence of substrate-specific active sites that could be optimized using structure-guided design.

## ■ ASSOCIATED CONTENT

### ■ Supporting Information

Detailed descriptions of peptide synthesis and characterization, kinetics, CD, and structure determination. Coordinates of the  $\beta$ Est-2C bundle have been deposited in the Cambridge Crystallographic Data Centre as entry CCDC 1000723. These data can be obtained free of charge at [www.ccdc.cam.ac.uk/data\\_request/cif](http://www.ccdc.cam.ac.uk/data_request/cif). This material is available free of charge via the Internet at <http://pubs.acs.org>.

## ■ AUTHOR INFORMATION

### Corresponding Author

alanna.schepartz@yale.edu

### Notes

The authors declare no competing financial interest.

## ■ ACKNOWLEDGMENTS

We are grateful to the W. M. Keck Foundation for support of this work and to Professor Scott Miller, Professor Anna Marie Pyle, and Dr. Clarissa Melo Czekster for helpful discussions. We are especially thankful to Professor Richard Baxter for providing laboratory space for peptide crystallization.

## ■ REFERENCES

- (1) (a) Davie, E. A. C.; Mennen, S. M.; Xu, Y. J.; Miller, S. J. *Chem. Rev.* **2007**, *107*, 5759. (b) Jacobsen, E. N.; MacMillan, D. W. C. *Proc. Natl. Acad. Sci. U.S.A.* **2010**, *107*, 20618. (c) Knowles, R. R.; Jacobsen, E. N. *Proc. Natl. Acad. Sci. U.S.A.* **2010**, *107*, 20678.
- (2) (a) Muller, M. M.; Windsor, M. A.; Pomerantz, W. C.; Gellman, S. H.; Hilvert, D. *Angew. Chem., Int. Ed.* **2009**, *48*, 922. (b) Coffey, P. E.; Drauz, K. H.; Roberts, S. M.; Skidmore, J.; Smith, J. A. *Chem. Commun.* **2001**, 2330.
- (3) (a) Appella, D. H.; Barchi, J. J.; Durell, S. R.; Gellman, S. H. *J. Am. Chem. Soc.* **1999**, *121*, 2309. (b) Hart, S. A.; Bahadoor, A. B. F.; Matthews, E. E.; Qiu, X. Y. J.; Schepartz, A. *J. Am. Chem. Soc.* **2003**, *125*, 4022. (c) Kritzer, J. A.; Stephens, O. M.; Guarracino, D. A.; Reznik, S. K.; Schepartz, A. *Bioorg. Med. Chem.* **2005**, *13*, 11. (d) Seebach, D.; Gardiner, J. *Acc. Chem. Res.* **2008**, *41*, 1366.
- (4) (a) Daniels, D. S.; Petersson, E. J.; Qiu, J. X.; Schepartz, A. *J. Am. Chem. Soc.* **2007**, *129*, 1532. (b) Goodman, J. L.; Petersson, E. J.; Daniels, D. S.; Qiu, J. X.; Schepartz, A. *J. Am. Chem. Soc.* **2007**, *129*, 14746. (c) Petersson, E. J.; Craig, C. J.; Daniels, D. S.; Qiu, J. X.; Schepartz, A. *J. Am. Chem. Soc.* **2007**, *129*, 5344. (d) Craig, C. J.; Goodman, J. L.; Schepartz, A. *ChemBiochem* **2011**, *12*, 1035.
- (5) Clark, D. D.; Boyd, J. M.; Ensign, S. A. *Biochemistry* **2004**, *43*, 6763.
- (6) (a) Ghosh, D.; Sawicki, M.; Lala, P.; Eрман, M.; Pangborn, W.; Eyzaguirre, J.; Gutierrez, R.; Jornvall, H.; Thiel, D. J. *J. Biol. Chem.* **2001**, *276*, 11159. (b) Osterlund, T.; Contreras, J. A.; Holm, C. *FEBS Lett.* **1997**, *403*, 259.
- (7) (a) Breslow, R. *Acc. Chem. Res.* **1995**, *28*, 146. (b) Li, X. Y.; Liu, D. R. *J. Am. Chem. Soc.* **2003**, *125*, 10188. (c) Cleij, M. C.; Drenth, W.; Nolte, R. J. M. *Recl. Trav. Chim. Pays-Bas* **1992**, *111*, 459. (d) Cleij, M. C.; Drenth, W.; Nolte, R. J. M. *Recl. Trav. Chim. Pays-Bas* **1993**, *112*, 1. (e) Javor, S.; Delort, E.; Darbre, T.; Reymond, J. L. *J. Am. Chem. Soc.* **2007**, *129*, 13238. (f) Broo, K. S.; Nilsson, H.; Nilsson, J.; Flodberg, A.; Baltzer, L. *J. Am. Chem. Soc.* **1998**, *120*, 4063. (g) Broo, K. S.; Nilsson, H.; Nilsson, J.; Baltzer, L. *J. Am. Chem. Soc.* **1998**, *120*, 10287. (h) Douat-Casassus, C.; Darbre, T.; Reymond, J. L. *J. Am. Chem. Soc.* **2004**, *126*, 7817. (i) Esposito, A.; Delort, E.; Lagnoux, D.; Djojo, F.; Reymond, J. L. *Angew. Chem., Int. Ed.* **2003**, *42*, 1381. (j) Kofoed, J.; Darbre, T.; Reymond, J. L. *Org. Biomol. Chem.* **2006**, *4*, 3268. (k) Delort, E.; Darbre, T.; Reymond, J. L. *J. Am. Chem. Soc.* **2004**, *126*, 15642. (l) Bolon, D. N.; Mayo, S. L. *Proc. Natl. Acad. Sci. U.S.A.* **2001**, *98*, 14274. (m) Wei, Y. N.; Hecht, M. H. *Protein Eng. Des. Sel.* **2004**, *17*, 67. (n) Baumeister, B.; Sakai, N.; Matile, S. *Org. Lett.* **2001**, *3*, 4229.
- (8) Getzoff, E. D.; Cabelli, D. E.; Fisher, C. L.; Parge, H. E.; Viezzoli, M. S.; Banci, L.; Hallewell, R. A. *Nature* **1992**, *358*, 347.
- (9) Vial, L.; Dumy, P. *J. Am. Chem. Soc.* **2007**, *129*, 4884.
- (10) For this initial series, we avoided using  $\beta^3$ -homohistidine due to challenges associated with its synthesis.
- (11) Petersson, E. J.; Schepartz, A. *J. Am. Chem. Soc.* **2008**, *130*, 821.
- (12) Reed, M. C.; Lieb, A.; Nijhout, H. F. *Bioessays* **2010**, *32*, 422.
- (13) Haldane, J. B. S. *Enzymes*; Longmans, Green: London and New York, 1930.
- (14) Uter, N. T.; Perona, J. J. *Proc. Natl. Acad. Sci. U.S.A.* **2004**, *101*, 14396.
- (15) (a) Goodman, J. L.; Molski, M. A.; Qiu, J.; Schepartz, A. *ChemBiochem* **2008**, *9*, 1576. (b) Wang, P. S. P.; Craig, C. J.; Schepartz, A. *Tetrahedron* **2012**, *68*, 4342.
- (16) Lee, D.; Lee, J.; Seok, C. *Phys. Chem. Chem. Phys.* **2013**, *15*, 5844.